Modal Analysis of Rectangular Waveguides with 2D Metamaterials

**Benedikt Byrne[1, 2, 3, *], Nathalie Raveu[1], Nicolas Capet[2],
Gwenn Le Fur[3], and Luc Duchesne[3]**

Abstract—A new method to rapidly design 2D metamaterials for rectangular waveguides by rebuilding their dispersion properties is proposed. The Modal Expansion Theory (MET) is revisited for theoretical surfaces with fixed surface impedances Z_S. Then, it is pursued for real dispersive anisotropic surfaces, which have surface impedances that are dependent on the frequency and the incidence angle. An algorithm which calculates the correct incidence angle of the guided electromagnetic mode at each frequency is presented. By including this algorithm in the MET and by combining it with a code based on the Finite Element Method (FEM) to calculate the surfaces impedances, dispersion diagrams of waveguides with real 2D anisotropic walls are correctly rebuilt. This is validated by comparing the results for two different metamaterials, corrugation- and T-structure, with those obtained using a commercial software.

1. INTRODUCTION

There are different possibilities to design metamaterials by describing their properties analytically. One is to define the volume by its relative permittivity ϵ_r and permeability μ_r. This has been used for the design of a metamaterial loaded waveguide with the aim to reduce the cutoff frequency [1–4] or to reduce the cross section as it was shown for miniaturized circular-waveguide probes [5]. Results are obtained here by homogenization (ϵ_r) of the metamaterial volume with consideration of the polarization anisotropy of the metamaterial. Another possibility is to describe metamaterials by their surface impedances at the height of the volume, as done in [6]. The latter characterization of the metamaterials is used in this paper. Thereby, the metamaterials can be optimised by means of a surface impedance condition. Placing the optimised metamaterials on the inner wall of horn antennas [7–9] permits the achievement of hard and soft horns.

In previous work [10], the development of the modal theory for propagation in structures with constant anisotropic surface impedances as boundary conditions has been developed for cylindrical waveguides and rectangular waveguides with vertical anisotropic surfaces. Here, these impedances are theoretical surface impedances which are independent of frequency. It allows a fast analysis of waveguides with all kinds of fixed isotropic and anisotropic surface impedances.

In this paper, the MET is extended for real 2D anisotropic surfaces in rectangular waveguides. Therefore, the surface impedances are defined on top of the volume, and the dependence of frequency f and incidence angle θ are taken into account. The anisotropic surfaces analysed in this paper consist of a corrugation and a T-structure ($h < \lambda_0/10$ or both, with λ_0 the operational wavelength).

2. CHARACTERIZATION PRINCIPLES

2.1. Modal Expansion Theory

In the following, the Cartesian coordinate system, cf. Figure 1, will be considered. In the horizontal sections ($y = 0$ and $y = b$), the walls are Perfect Electric Conductors (PEC), while the vertical sections ($x = 0$ and $x = a$) are constant surface impedances $Z_S|_{x=0} = Z_S|_{x=a}$.
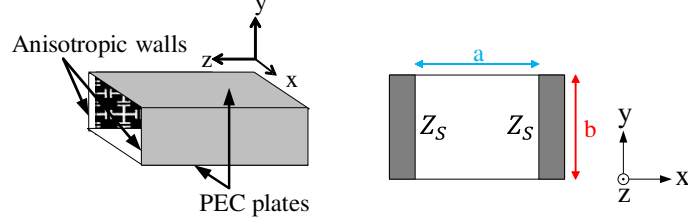

Figure 1. Rectangular waveguide with anisotropic surfaces on the vertical walls.

The boundary conditions are expressed at the limits of the waveguide ($x = 0$, $x = a$, $y = 0$ et $y = b$).

- On vertical walls, the anisotropic surface impedance conditions are:

$$Z_t = \left.\frac{E_y}{H_z}\right|_{x=0} = -\left.\frac{E_y}{H_z}\right|_{x=a}, \tag{1}$$

$$Z_z = -\left.\frac{E_z}{H_y}\right|_{x=0} = \left.\frac{E_z}{H_y}\right|_{x=a}. \tag{2}$$

Z_t and Z_z are complex, since losses can be present. However, the examples treated here are lossless.

- On horizontal walls, the condition is metallic, hence, the boundary conditions are:

$$0 = E_z|_{y=0} = E_z|_{y=b}, \quad 0 = \left.\frac{\partial H_z}{\partial y}\right|_{y=0} = \left.\frac{\partial H_z}{\partial y}\right|_{y=b}. \tag{3}$$

For this kind of rectangular waveguide, the dispersion equation is obtained [10]:

$$0 = 2K_{zyc}^2 z_z \left[-z_t + \frac{X+1}{1-X} K_{0xc}\left(z_z z_t + 1\right) - K_{0xc}^2 z_z \right] + \left(K_{zyc}^4 + K_{0xc}^4\right) z_z^2 - 2K_{0xc}^3 \frac{X+1}{1-X} z_z \left(z_z z_t + 1\right)$$

$$+ K_{0xc}^2 \left[1 + (z_z z_t)^2 + 4\left(\frac{X+1}{1-X}\right)^2 z_z z_t \right] - 2K_{0xc} \frac{X+1}{1-X} z_t \left(1 + z_z z_t\right) + z_t^2, \tag{4}$$

with $X = e^{-2jk_x a}$, the constants $K_{0xc} = (k_0 k_x)/k_c^2$, $K_{zyc} = (\gamma_z k_y)/k_c^2$ and z_z, z_t the normalized surface impedances ($z_z = Z_z/Z_0$ and $z_t = Z_t/Z_0$), with Z_0 the characteristic impedance. k_0 is the propagation constant in vacuum, k_c the cutoff constant, and k_x, k_y and γ_z are the wave propagation constants in x, y and z directions, respectively. Equation (4) is a function of the propagation constant in the form $f(k_c) = 0$. It is solved numerically.

In this study, we are interested in the first modes propagating in waveguides, which generally have the index $m = 0$ ($k_y = 0$). For this case, the dispersion equation has to be analysed separately [10]:

$$k_c^2 z_t^2 (1 - X) - 2k_0 k_c z_t (1 + X) + k_0^2 (1 - X) = 0 \quad \text{and} \quad X = e^{-j2k_c a}. \tag{5}$$

It can be noticed that this equation, valid for $m = 0$, is indeed deduced from the general Equation (4) and is independent of z_z. We have $K_{zyc} = 0$ since $k_y = 0$, and $K_{0xc} = \frac{k_0}{k_c}$ since $k_x = k_c$. By inserting these values in Equation (4) and multiplying the equation by $(1 - X)$, we obtain Equation (5). The mode type can be determined by observing k_x. When $k_x = 0$, the mode type is TEM, and otherwise, the mode type is TE.

2.2. MET for Metamaterials

In the case of a metamaterial, the surface impedances Z'_t and Z'_z are calculated above the partially metalized volume of height h. These values of the surface impedances, used in the MET, have to be calculated at each frequency separately. Beside the frequency dependence, Z'_t and Z'_z are also dependent on the incidence angles θ and ϕ. Since this paper is about 2D metamaterials, only the angle θ is considered here, c.f. Figure 2.

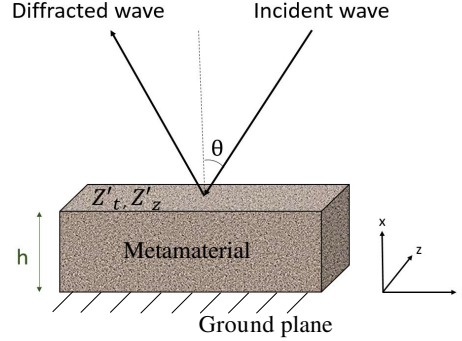**Figure 2.** Definition of the surface impedances seen at a height h of an anisotropic surface with a dependency on the incidence angle θ.

2.2.1. Scheme of the Recursive Solution

To illustrate the dependence of the surface impedances to the incidence angle θ, an example of dispersion diagram of a rectangular waveguide ($a = 22.86\,\text{mm}$, $b = 10.16\,\text{mm}$) with isotropic surface impedances $Z_t = Z_z = jZ_0$ on its vertical walls is presented in Figure 3(a), with $\epsilon_{eff} = (Im(\gamma_z)/k_0)^2$.
   Results obtained with the electromagnetic software HFSS (High Frequency Structure Simulator) from Ansys (black circles) represent dispersion curve of the fundamental mode propagating in this waveguide and are the reference to which the MET results shall be compared. For the other two curves, the first step was to compute the surface impedances in HFSS by using a unit cell of the surface ($Z_t = Z_z = jZ_0$) with periodic boundaries and a Floquet port excitation. The surface impedances are calculated at a height over the isotropic surface ($h = 2\,\text{mm}$) by taking into account their frequency variation ($Z'_t(f, \theta)$, $Z'_z(f, \theta)$). However, two fixed angles θ ($0°$ and $89°$) have been chosen. These curves (red and blue dots) have then been calculated with the MET code by using these surface impedances.
   By analysing the three curves, it can be noticed around the cutoff frequency that the dispersion curve calculated with HFSS is closer to the MET curve with $\theta = 0°$. On the other hand, at higher frequencies, it is closer to the MET curve with $\theta = 89°$. Hence, we have an evolution of θ as a function of the frequency in between the cutoff frequency and the higher frequencies from $0°$ to $89°$, respectively. Beside their frequency dependence, the surface impedances are, thus, also dependent on the incidence angle θ, which, a priori, is unknown for a given mode. Hence, this angle has to be corrected at each frequency separately and for each mode.
   According to Figure 2, the propagation constants are given by

$$k_x = k_0 \cos\theta, \quad k_y = 0, \quad \gamma_z = j\beta = jk_0 \sin\theta. \tag{6}$$

Hence, the angle θ can be written as:

$$\theta = \sin^{-1}\left(\frac{\beta}{k_0}\right) \tag{7}$$

Now, according to Eq. (7), the angle θ is related to the propagation constant β. The angle θ can thus be calculated iteratively for each frequency. At the cutoff frequency, the incidence angle is normal to the surface ($\theta = 0°$), then, it evolves with the frequency, up to oblique angles. Knowing the propagation constant β at the previous frequency, the new initial θ_0 of the actual frequency is found. The solution of the MET gives the corresponding β. If the new value of θ (θ_{new}) is correct, β correlates with it. If not,
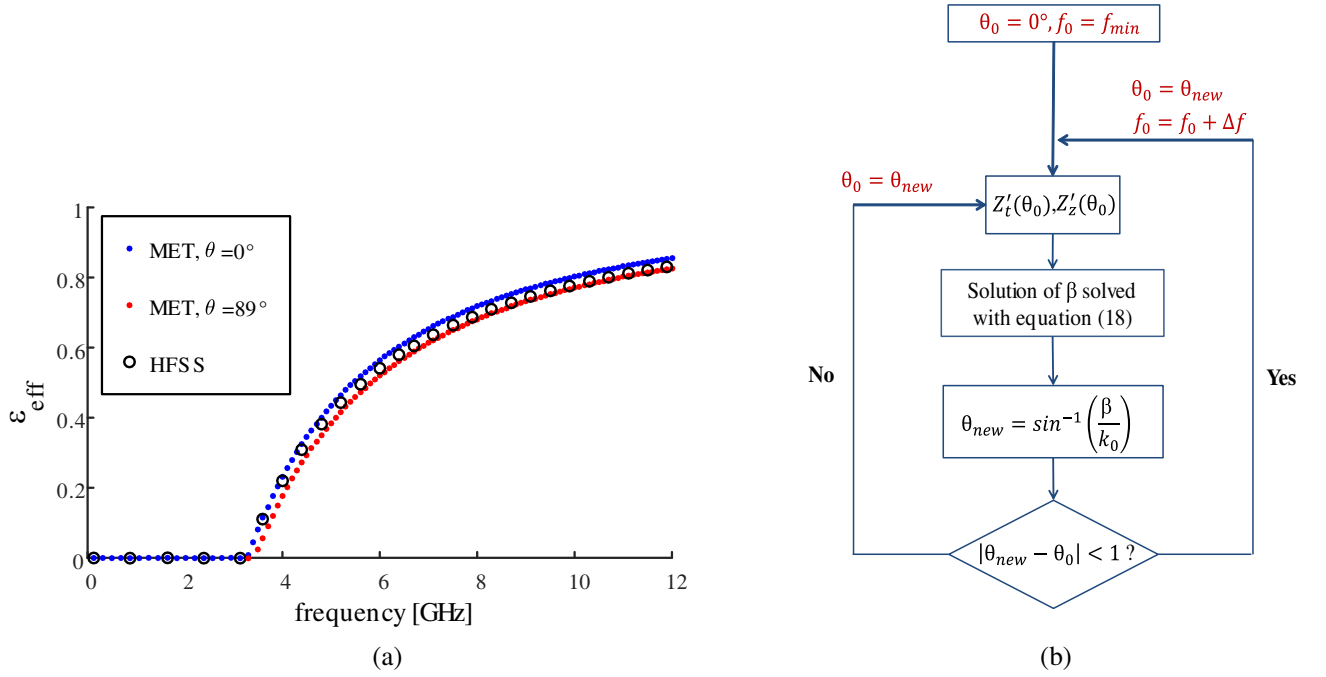
Figure 3. (a) A dispersion diagram example that shows the dependency of the dispersion properties to the angle θ and (b) a schematic algorithm to correct the angle θ.

$\theta_0 = \theta_{new}$ has to be modified, which yields a modification of the values Z'_t and Z'_z and hence a new β. This procedure is repeated as long as the difference between the two angles, computed at two successive iterations, is larger than a precision defined by the user. The algorithm is illustrated in Figure 3(b).

By using the algorithm of Figure 3(b) in the MET code, the dispersion diagram of surfaces with a certain height h for modes with $m = 0$ can be rebuilt very rapidly. To demonstrate the validity, the MET code has been used for isotropic surfaces $Z_t = Z_z = jZ_0$ and $Z_t = Z_z = -jZ_0$. This time, the correction of θ at each frequency has been included. The results are illustrated in Figures 4(a) and 4(b) for the surfaces $Z_t = Z_z = jZ_0$ and $Z_t = Z_z = -jZ_0$, respectively. The dispersion curves are now coinciding very well with the HFSS results. In Figure 4(b), it can be seen that at certain frequencies the angle θ has complex values, in the form of $\theta = (90 - jx)$. More precisely, θ gets complex for effective permittivities ϵ_{eff} higher than 1, thus, $\beta > k_0$, since $\epsilon_{eff} = (\beta/k_0)^2$. An explanation of the merging of these complex angles is described below.

2.2.2. Physical Analysis of the Signification of Complex Values of θ

For two dimensions and hence for modes with cancelled propagation constant in y direction ($k_y = \frac{m\pi}{b} = 0$), the relation between the propagation constants β and k_x can be written as:

$$\beta^2 = k_0^2 - k_x^2. \tag{8}$$

If $\beta \leq k_0$, a vectorial construction of the propagation constants as represented in Figure 5(a) is possible. For a metallic waveguide for example, this vectorial construction is always true. Hence, the propagation constants are described in z direction with

$$\beta = k_0 \sin \theta < k_0 \tag{9}$$

and in x direction with

$$k_x = k_0 \cos \theta < k_0. \tag{10}$$

Now, if $\beta > k_0$ and hence $k_x^2 < 0$, the propagation constant in x direction is purely imaginary. Thus, $k_x = j\alpha_x$, with $\alpha_x \in \mathbb{R}$. With the help of Figure 5(b), it can be stated that a direct construction in
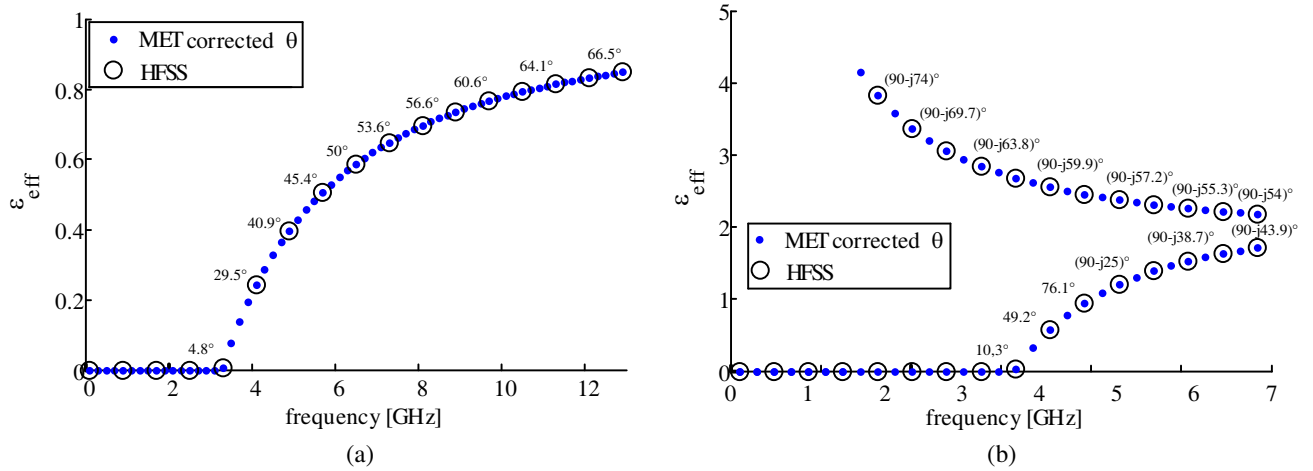
Figure 4. Dispersion diagrams of rectangular waveguides with isotropic surfaces (a) $Z_t = Z_z = jZ_0$ and (b) $Z_t = Z_z = -jZ_0$ on the vertical walls calculated with the MET with the correction of θ.
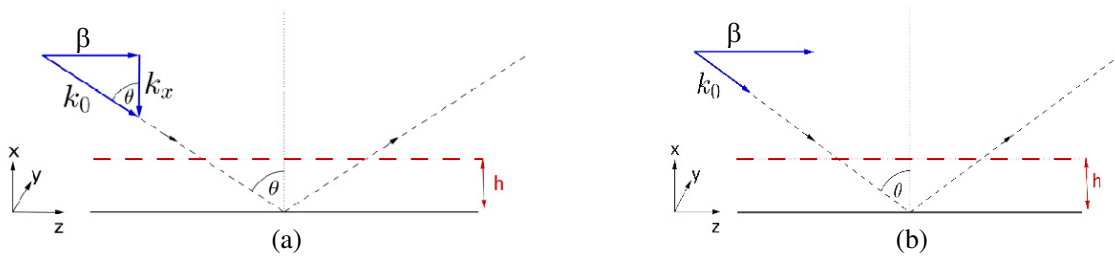

Figure 5. Vectorial construction of the propagation constants for a reflected plane wave on a 2D surface.

vectorial form of the propagation constants is not possible anymore. The angle θ does not have any physical meaning anymore. Anyway, it is possible to determine β by using complex angles θ. Even if the complex incidence angle θ does not correspond to a physical incidence, Equation (7) is used in the MET code to rebuild the dispersion curves of waveguides with anisotropic walls. Consequently, it is necessary to include complex angles θ in the computation of the surface impedances. Currently, no commercial software is able to compute surface impedances by using complex incidence angles, which explains the suitability of developing an own FEM code. In the following section, this 2D FEM code, which enables the calculation of surface impedances Z'_t and Z'_z at each frequency whatever the angle θ, complex values included is presented.

2.3. Computation of the surface impedances with the FEM code

A representation of the unit cell of a 2D anisotropic surface is illustrated in Figure 6. For a better understanding, a corrugation has been chosen to represent the anisotropic surface in this figure. An incident electromagnetic wave, invariant in $\vec{y}$ and independent of y, is assumed. Ω' $(x = 0)$ is the level at which the surface impedances of the anisotropic structure (height h) are to be computed. Γ_S is the physical surface, which is defined as a perfect electric conductor here. Γ_1 and Γ_2 are the periodic boundaries of the unit cell. At level Γ_3, Floquet modes TE and TM are excited.

For <u>TE modes</u>, the following variables are defined:

$$E_{iy} = u_i, \quad E_{ry} = u_d. \tag{11}$$

Here, E_{iy} is the incident electric field, with

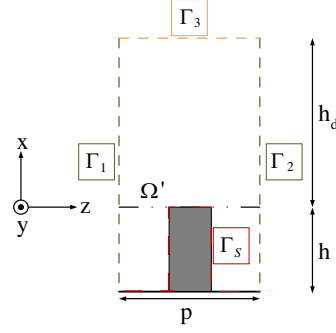$$u_i = -e^{jk_0 \sin\theta z} e^{jk_0 \cos\theta x} \tag{12}$$

Figure 6. Unit cell for the FEM computation of the surface impedances.

and E_{ry} is the diffracted electric field which constitutes the unknown variable. $u = u_i + u_d$ corresponds to the total field. The problem to solve is given in the following Equations (13)–(16). The equation of propagation is given by Eq. (13). The definition of the periodic walls is denoted in Eq. (14), the one of the surface impedance in Eq. (15). Eventually, Equation (16) presents the decomposition of the Floquet modes.

$$\nabla^2 u_d(x, z) + k_0^2 u_d(x, z) = 0, \tag{13}$$

$$u_d|_{\Gamma_1} = u_d|_{\Gamma_2}, \tag{14}$$

$$u|_{\Gamma_S} = \frac{-Z_S}{j\omega\mu_0} \frac{\partial u}{\partial n}\bigg|_{\Gamma_S} = \frac{-Z_S}{j\omega\mu_0} \left(\frac{\partial u_d}{\partial n}\bigg|_{\Gamma_S} + \frac{\partial u_i}{\partial n}\bigg|_{\Gamma_S} \right), \tag{15}$$

$$u_d|_{\Gamma_3} = \sum u_n e^{j\gamma_n z} e^{\alpha_n p}, \tag{16}$$

with n the normal vector to Γ_S, μ_0 the vacuum permeability, p the distance between the periodic boundaries of the unit cell, $\gamma_n = -k_0 \sin\theta + \frac{2\pi n}{p}$ and $\alpha_n = \sqrt{\gamma_n^2 - k_0^2}$.

By using the FEM and hereby developing the equations for E_y and H_z, as described in [12], the surface impedance of the TE mode at Ω' can be calculated with

$$Z_t = -\frac{E_y}{H_z}\bigg|_{\Omega'}. \tag{17}$$

For <u>TM modes</u>, the equations to calculate the surface impedance Z_z with the aid of a unit cell, as in Figure 6, are developed similarly. This time, the incident and diffracted variables are:

$$H_{iy} = u_i, \quad H_{ry} = u_d, \tag{18}$$

with H_{iy} the incident magnetic field (known) and:

$$u_i = -e^{-jk_0 \sin\theta z} e^{jk_0 \cos\theta x}. \tag{19}$$

H_{ry} is the diffracted magnetic field, which is the unknown of the problem.

As for the TE mode, the propagation Equation (13), conditions of periodicity in Eq. (14), Floquet modes decomposition in Eq. (16) are to be solved. To these equations the condition on Γ_S, which is given by 20, is joined.

$$u|_{\Gamma_S} = -j\omega\epsilon_0 Z_S \frac{\partial u}{\partial n}\bigg|_{\Gamma_S} = -j\omega\epsilon_0 Z_S \left(\frac{\partial u_d}{\partial n}\bigg|_{\Gamma_S} + \frac{\partial u_i}{\partial n}\bigg|_{\Gamma_S} \right), \tag{20}$$

with ϵ_0 the vacuum permittivity. Eventually [12], the surface impedance seen by the TM mode at Ω' can be solved with:

$$Z_z = \frac{E_z}{H_y}\bigg|_{\Omega'}. \tag{21}$$

3. RESULTS

In order to validate the FEM approach included in the MET code, two structures of metamaterials have been chosen: a corrugation and a T-structure. Both structures are arranged longitudinally to the direction of propagation, so as to be invariant in y direction. The mesh structures of the surfaces are defined in the open source software Gmsh [11]. The meshing is then used in the FEM code. The structures and the used mesh of the corrugation and T-structure are illustrated in Figures 7(a) and 7(b), respectively. For the corrugation, the dimensions are $h = 18.2\,\text{mm}$, $h_d = h$, $p = 26.225\,\text{mm}$ and $t = 5.425\,\text{mm}$. For the T-structure, they are $h = 4.55\,\text{mm}$, $h_d = h$, $p = 4\,\text{mm}$, $t = 0.5\,\text{mm}$ and $q = 3.5\,\text{mm}$.

The computed surface impedances with the FEM are then used in the MET code to calculate the dispersion properties. The results of two different waveguides with the anisotropic surfaces described above on the vertical walls are compared to HFSS results. For the HFSS results, dispersion diagrams have been obtained from a section of a given waveguide using periodic boundary conditions, as shown in Figure 8. For a given propagation constant, which is a function of the phase delay between two periodic boundary conditions and the distance p between them, the eigenmode solver of HFSS returns the frequency of each solution. By varying the phase delay between the two periodic boundary conditions from $0°$ to $180°$, the complete dispersion diagram of the guided structure can be obtained.

For the corrugation, a waveguide of dimensions $a = 163.6\,\text{mm}$ and $b = 100\,\text{mm}$ is chosen. The dispersion diagram is represented in Figure 9(a). The first two modes with the index $m = 0$ (TE_{10} and TE_{20}) have been calculated by the MET code (blue dots). The code takes $11\,\text{s}$ to compute the
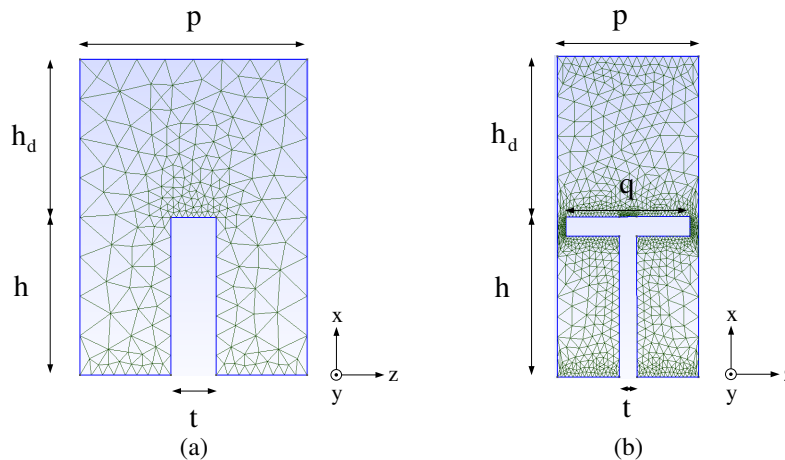

Figure 7. Unit cells and their meshs defined with Gmsh.
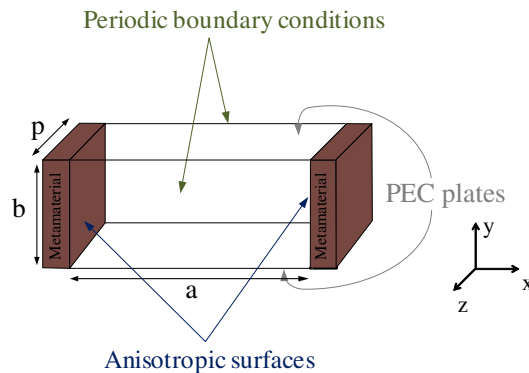

Figure 8. Representation of the waveguide with its periodic boundary conditions and anisotropic surfaces simulated in HFSS.

dispersion diagram with the two modes with a Intel Core i7 (3.6 GHz, 8 GB of RAM) processor. The same modes obtained with HFSS (red stars) have been added to the diagram and coincide perfectly. However, the computation takes 547 s and is therefore 50 times slower than the MET code by using the same processor.

For the T structure, the dimensions of the waveguide are $a = 22.9$ mm and $b = 16$ mm. The dispersion diagram of the waveguide with T-structure on the vertical walls calculated by the MET code is illustrated in Figure 9(b). Here again, the HFSS curves have been added to the MET results, and the two overlap completely. The simulation time (Intel Core i7, 3.6 GHz, 8 GB of RAM) with the MET code is 112 s to compute the dispersion diagram, whereas the one with HFSS is 365 s (3.3 times slower than MET code). The time difference between the MET computation of the corrugation and the T-structure is due to the higher number of tetrahedrons in the meshing of the T-structure, which is visible in Figure 7 (993 nodes for the T-structure in comparison to 233 nodes for the corrugation).
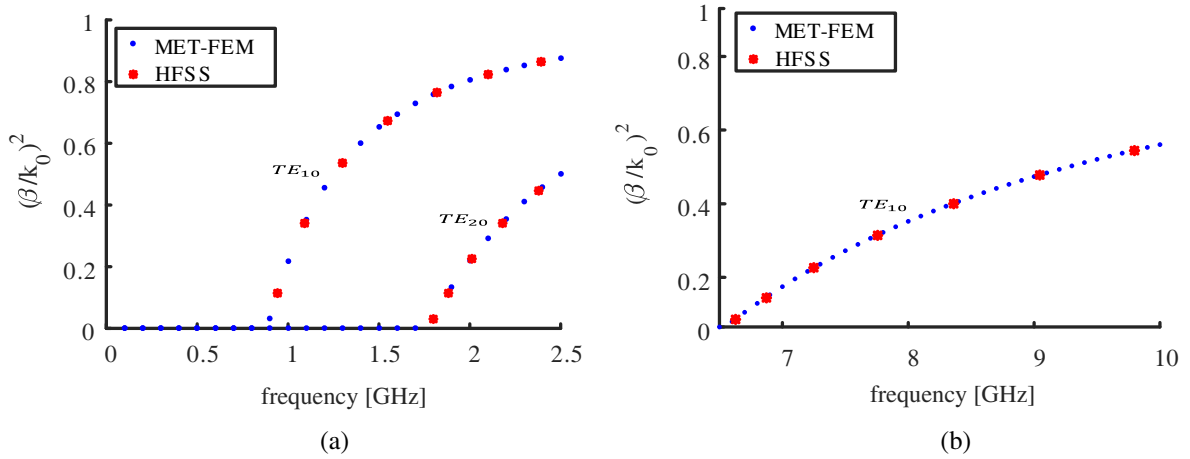

(a)   (b)

Figure 9. Dispersion diagrams of rectangular waveguides with a (a) corrugation- and (b) T-surface by using the meshing illustrated in Figure 7.

The dispersion properties of any other 2D metamaterial structure employed in this kind of rectangular waveguides can be analysed with the MET method introduced in this article.

4. CONCLUSION

A new method based on the Modal Expansion Theory and with the obective of computing the dispersion properties of waveguides with 2D metamaterials has been developed. Two anisotropic surfaces (corrugation and metamaterial), invariant in y direction, embedded in a rectangular waveguide have been tested and have demonstrated the efficiency of the proposed tool in matters of accuracy and time. This method is planned to be further developed for 3D metamaterials. To do so, the FEM shall be developed for 3D metamaterials and the incidence angle ϕ shall be corrected.

REFERENCES

1. Pollock, J. G. and A. K. Iyer, "Below-cutoff propagation in metamaterial-lined circular waveguides," *IEEE Trans. Microw. Theory Techn.*, Vol. 61, No. 9, 3169–3178, September 2013.
2. Pollock, J. G. and A. K. Iyer, "Experimental verification of below-cutoff propagation in miniaturized circular waveguides using anisotropic ENNZ metamaterial liners," *IEEE Transactions n Microwave Theory and Techniques*, Vol. 64, No. 4, 1297–1305, April 2016.
3. Capolino, F., *Applications of Metamaterials*, CRC Press, ISBN 9781420054231, 2009.
4. Engheta, N. and R. W. Ziolkowski, *Metamaterials: Physics and Engineering Explorations*, Wiley-IEEE Press, ISBN 9780471761020, 2006.

5. Pollock, J. G. and A. K. Iyer, "Miniaturized circular-waveguide probe antennas using metamaterial liners," *IEEE Trans. Antennas Propag.*, Vol. 63, No. 1, 428–433, January 2015.

6. Wu, Q., M. D. Gregory, D. H. Werner, P. L. Werner, and E. Lier, "Nature-inspired design of soft, hard and hybrid metasurfaces," *2010 IEEE Antennas and Propagation Society International Symposium (APSURSI)*, 1–4, Toronto, Canada, July 2010.

7. Lier, E., "Review of soft and hard horn antennas, including metamaterial-based hybrid-mode horns," *IEEE Antennas Propagat. Mag.*, Vol. 52, No. 2, 31–39, April 2010.

8. Lier, E. and R. K. Shaw, "Design and simulation of metamaterial-based hybrid-mode horn antennas," *Electron. Lett.*, Vol. 44, No. 25, 1444–1445, December 2008.

9. Kildal, P. S., "Artificially soft and hard surfaces in electromagnetics and their application to antenna design," *Proc. 23rd Eur. Microw. Conf.*, 30–33, September 1993.

10. Raveu, N., B. Byrne, L. Claudepierre, and N. Capet, "Modal theory for waveguides with anisotropic surface impedance boundaries," *IEEE Transactions on Microwave Theory and Techniques*, Vol. 64, No. 4, 1153–1162, April 2016.

11. Geuzaine, C. and J.-F. Remacle, "Gmsh: A three-dimensional finite element mesh generator with built-in pre- and post-processing facilities," *International Journal for Numerical Methods in Engineering*, Vol. 79, No. 11, 1309–1331, 2009.

12. Jin, J.-M., "The finite element method in electromagnetics," 3rd Edition, Wiley-IEEE Press, ISBN 978-1-118-57136-1, 2014.